PHILOSOPHICAL MAGAZINE, 1 September 2003
VOL. 83, NO. 25, 2941–2953

Taylor & Francis
Taylor & Francis Group

Intrinsic nanoscale phase separation of bulk As_2S_3 glass

D. G. GEORGIEV, P. BOOLCHAND†

Department of Electrical, Computer Engineering and Computer Science,
University of Cincinnati, Cincinnati, Ohio 45221-0030, USA

and K. A. JACKSON

Department of Physics, Central Michigan University,
Mount Pleasant, Michigan 48858, USA

[*Received 27 April 2003 and accepted 20 May 2003*]

ABSTRACT

Raman scattering on bulk As_xS_{1-x} glasses shows that vibrational modes of As_4S_4 monomer first appear near $x=0.38$, and their concentration increases precipitously with increasing x, suggesting that the stoichiometric glass ($x=0.40$) is intrinsically phase separated into small As-rich (As_4S_4) and large S-rich clusters. Support for the Raman-active vibrational modes of the orpiment-like and realgar-like nanophases is provided by *ab-initio* density functional theory calculations on appropriate clusters. Nanoscale phase separation provides a basis for understanding the global maximum in the glass transition temperature T_g near $x=0.40$, and the departure from Arrhenius temperature activation of As_2S_3 melt viscosities.

§1. INTRODUCTION

Orpiment (As_2S_3) crystallizes in a layer-like structure with each layer consisting of 12-membered $As_2(S_{1/2})_3$ rings (Morimoto 1954) (see also Renninger *et al.* (1973)), forming elements of medium-range structure. Each ring consists of six pyramidally coordinated $As(S_{1/2})_3$ units with bridging S atoms. The *intralayer* bonding interactions are covalent, while the *interlayer* interactions are van der Waals in character and weaker. The vibrational density of states in orpiment has been examined by Raman scattering (Zallen and Slade 1974, Kawamura *et al.* 1983). Interlayer optic modes exhibit pressure shifts (Zallen 1974) at least an order of magnitude larger (Grüneisen mode) than intralayer modes, confirming the quasi-two-dimensional molecular structure in vibrational spectroscopy.

In analogy to orpiment the molecular structure of stoichiometric As_2S_3 glass is widely regarded to consist of a network of S-bridging pyramidal $As(S_{1/2})_3$ units (Myers and Felty 1967). Several studies have emphasized that the similarity of structure goes beyond the local order to the medium-range order; that is, the glass network also possesses a layer-like structure (Tanaka *et al.* 1985, Tanaka 1989, Shimakawa *et al.* 1998, Taylor *et al.* 1998) although that view is not shared

† Author for correspondence. Email: pboolcha@ececs.uc.edu.

Philosophical Magazine ISSN 1478–6435 print/ISSN 1478–6443 online © 2003 Taylor & Francis Ltd
http://www.tandf.co.uk/journals
DOI: 10.1080/1478643031000151196

universally (Yang *et al.* 1987). Evidence for presence of a small but finite (less than 2%) concentration of like-atom bonds (As–As and S–S) in the stoichiometric glass has emerged from Raman scattering (Frumar *et al.* 1997, Wagner *et al.* 1998) and ^{129}I Mössbauer spectroscopy (Zitkovsky 1989).

An issue of central importance concerns the distribution of these like-atom bonds in the glass structure. A common view is to regard such bonds as 'defects' in a fully polymerized network. The like-atom bonds then form at random in a nearly chemically ordered but continuous random network. An alternative view (Phillips *et al.* 1980) is to regard the As–As bonds and S–S bonds as forming part of two distinct molecular clusters which bond to each other by weaker (van der Waals) forces. In the latter model, internal surfaces become an intrinsic feature of glass structure and the network is viewed as partially polymerized, that is phase separated on a molecular scale or nanoscale.

Nanoscale phase separation effects are of general interest in glass science (Boolchand *et al.* 2002). Such structural effects usually produce pronounced changes in glass physical properties including a lowering of the glass transition temperature, a lowering of the optical bandgap and an increase in molar volumes as network global connectivity diminishes. These pronounced changes in physical properties can mask the more subtle elastic effects related to rigidity transitions as discussed recently (Boolchand *et al.* 2002). In general, it appears that chalcogen-rich glasses are usually fully polymerized, but chalcogen-deficient glasses tend to demix into characteristic nanophases although exceptions do occur. Stoichiometric glasses (GeS_2, $GeSe_2$, As_2Se_3 and As_2S_3) that are at the boundary between chalcogen-rich and chalcogen-deficient glasses have thus attracted much attention. The evidence (Bresser *et al.* 1981) (see also Boolchand (2000a) and Boolchand and Bresser (2000)) suggests that the stoichiometric glasses of $GeSe_2$ and GeS_2 are composed of an anionic-rich majority phase and a cation-rich minority phase.

In this work, we present new Raman scattering and temperature-modulated differential scanning calorimetry (DSC) results on binary As_xS_{1-x} glasses focusing near the stoichiometric composition with $x = 2/5$. The present results in conjunction with previous ^{129}I Mössbauer effect results (Zitkovsky 1989) show that the stoichiometric As_2S_3 glass is nanoscale phase separated into small As_4S_4 molecules and compensating large S-rich clusters (Phillips *et al.* 1980). The finding is consistent with the global maximum of T_g near the stoichiometric composition, and the non-Arrhenius temperature activation of As_2S_3 liquid viscosities (Vinogradova *et al.* 1967) (see also Angell (1988, 1991)).

§ 2. Experimental results

99.999% As_2S_3 and elemental S and As lumps from Cerac, Inc., were used as starting materials to synthesize the S-rich ($x < 0.40$) and As-rich ($x > 0.40$) bulk As_xS_{1-x} glasses. All weighings were performed in a pure and dry N_2 ambient. The starting materials sealed in evacuated (5×10^{-7} Torr) quartz tubings were slowly reacted by heating to 700°C, and melts homogenized by continuous rocking in a furnace for 48 h. Melt temperatures were then slowly lowered to $T_\ell + 50$°C and melts equilibrated for several hours before a water quench. Glass transition temperatures $T_g(x)$ were measured using a model 2920 temperature-modulated DSC instrument from TA Instruments, at a $3^\circ C^{-1}$ min scan rate (heating followed by cooling) and a 1°C per 100 s modulation rate. $T_g(x)$ trends show an increase with increasing As content of the glasses at low x and a global maximum near $x = 0.40$, as shown

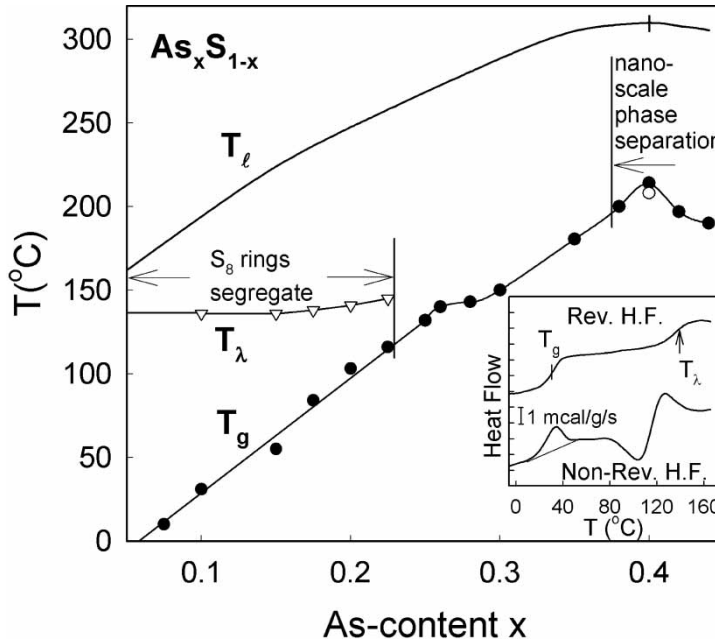

Figure 1. Compositional trends in glass transition temperature T_g and liquidus temperature T_l showing a global maximum near $x = 0.40$ in the titled binary. The inset shows the modulated DSC traces of the reversing heat flow (Rev. H.F.) and the non-reversing heat flow (Non-Rev. H.F.) of a sample at $x = 0.10$ with $T_g = 38^\circ C$ and the S polymerization transition temperature T_λ near 140°C.

in figure 1. The observed $T_g(x)$ trend closely parallels those of $T_\ell(x)$ (figure 1). Furthermore, $T_g(x)$ of a stoichiometric glass, melt quenched from $T_q = 550^\circ C$ (figure 1, open circle) is found to be 6°C lower than that of a sample melt quenched from $T_q = 350^\circ C$ (figure 1, full circles). Raman scattering excited by 6 mW of the 647.1 nm radiation from a Kr-ion laser, focused to a 50 μm spot size, was studied in a back-scattering geometry. The scattered radiation was analysed using a triple-monochromator system (model T64000 from Instruments SA, Inc.) and a charge-coupled device detector.

Figure 2 (*a*) shows Raman spectra of As_2S_3 glass samples synthesized at three different T_q values. The scattering strengths of the three modes labelled R in the $150\,cm^{-1} < \bar{\nu} < 250\,cm^{-1}$ range are found to increase steadily with increasing T_q. Furthermore, in the main band centred near $340\,cm^{-1}$, a feature near $360\,cm^{-1}$ becomes more conspicuous with increasing T_q. This group of modes labelled R in the glasses represent the realgar-like nanophase which consists of As_4S_4 molecules. Spectra of glasses near $x = 0.40$ are shown in figure 2 (*b*). Of special interest is the R mode at $190\,cm^{-1}$, which is not observed at $x = 0.35$ (see inset of figure 2 (*b*)) but first appears near $x = 0.38$ and is found to grow monotonically in scattering strength with increasing x thereafter.

Figure 3 compares Raman spectra of orpiment and realgar (β-As_4S_4) with those of glasses with $x = 0.40$ and 0.44. The realgar sample was synthesized by annealing an As_4S_4 melt for 72 h at $T_\ell = 25^\circ C$ followed by an air quench, and the nature of the crystalline phase (β-As_4S_4) ascertained by powder X-ray diffraction measurements. The Raman spectra of these crystalline phases are in excellent accord with earlier

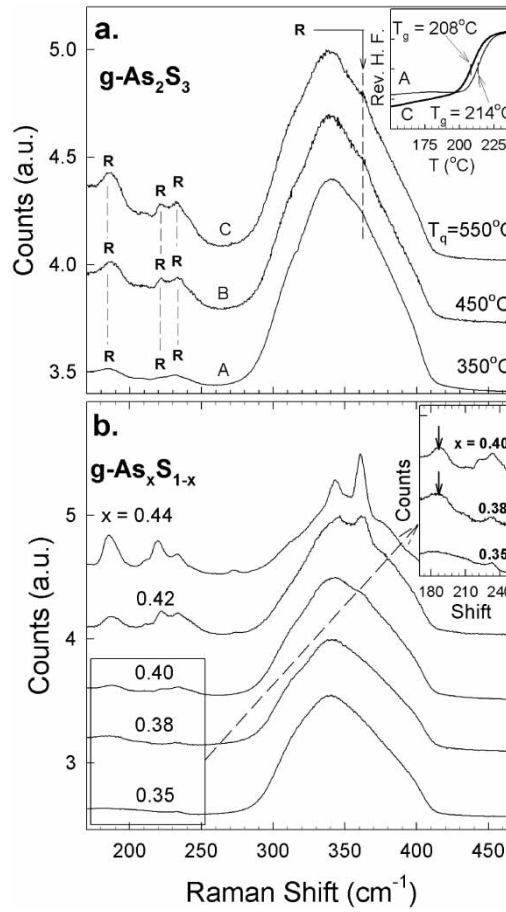

Figure 2. (*a*) Raman scattering of As_2S_3 glass samples quenched from the indicated melt temperatures T_q showing growth in scattering of the modes labelled R with T_q (a.u., arbitrary units). The inset shows the reduction in T_g from 214 to 206°C when T_q is increased from 350 to 550°C (Rev. H.F., reversing heat flow). (*b*) Raman scattering in binary As_xS_{1-x} glasses at indicated x showing the onset of the R modes at $x = 0.38$ (a.u., arbitrary units). The inset shows a magnified view of the R modes. The mode at 185 cm^{-1} at the arrow location onsets near $x = 0.38$.

reports (Kobliska and Solin 1973, Ward 1968, Miniz-Miranda *et al.* 1996). Figure 3 reveals that the narrow set of modes labelled R and observed in realgar have close parallels in the spectra of the glasses. On the other hand, the sharp modes seen in orpiment and labelled O, also have close parallels in the spectra of the glasses, except that they are blue-shifted by about 18 cm^{-1} and significantly broadened in the disordered phase.

§ 3. Discussion

3.1. *Raman mode assignments*

Our interpretation of these Raman results is as follows. The set of sharp modes labelled R in the glasses are traced to the presence of As_4S_4 monomers in the glasses. These intracage bond-stretching mode frequencies in realgar and those in the glasses

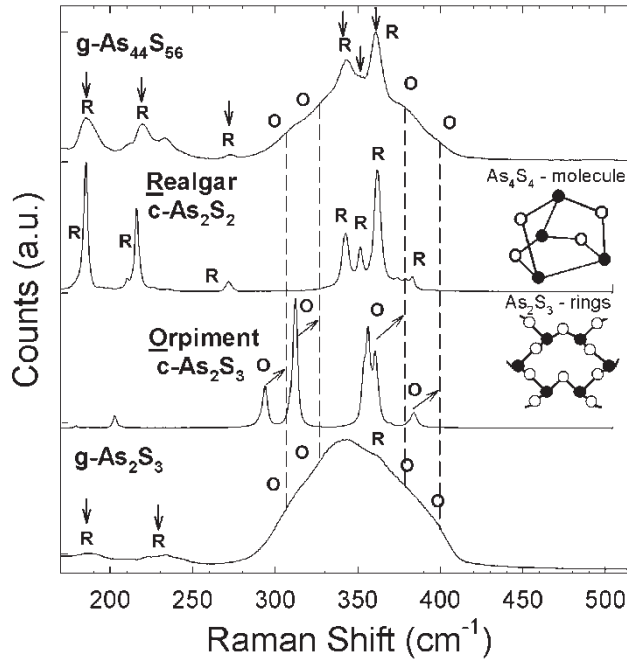

Figure 3. Raman scattering in the two crystalline phases, orpiment (crystalline As_2S_3) and realgar (β-As_4S_4) compared with the line shapes observed in the two indicated glasses at $x = 0.44$ and 0.40 (a.u., arbitrary units). Features labelled R in the glasses are identified with modes of realgar, while features labelled O in the glasses are identified with modes of orpiment. The orpiment modes in the glasses are blue-shifted by $18\,cm^{-1}$ and broadened in relation to the crystalline phase. See text for details.

are the same (within $\pm 5\,cm^{-1}$) because the cages are largely decoupled from the host networks. The R modes in glasses are broadened in relation to those in the crystal because of the presence of packing stresses in the disordered phase. The modes labelled O in the glasses are identified with pyramidal $As(S_{1/2})_3$ units that probably form rings whose size is less certain. The $18\,cm^{-1}$ blue shift of the O modes between orpiment and the glasses reflects a transfer of bonding strength from interlayer (van der Waals) interactions to intralayer (covalent) interactions due to loss in planarity of the layers in the glasses. A parallel example occurs in Se, where the bond stretching mode at $233\,cm^{-1}$ in trigonal Se is known to upshift to $250\,cm^{-1}$ in Se glass due to the more molecular nature of chains in the disordered phase (Zallen and Lucovsky 1976). The O modes are broadened in glasses because $As(S_{1/2})_3$ units are optimally constrained and can therefore distort, in sharp contrast with modes of $Ge(S_{1/2})_4$ tetrahedra that continue to be narrow in glasses because of the overconstrained nature of tetrahedra, and therefore less amenable to distortion.

3.2. *Density functional theory calculations on clusters*

The strong similarity between the $As_{0.44}S_{0.56}$ glass and crystalline As_4S_4 spectra (i.e. c-$As_{0.5}S_{0.5}$ or c-As_2S_2) shown in figure 3 is compelling evidence for the formation of As_4S_4 monomer units in the glass. To support this conclusion further, we have performed first-principles calculations based on the density functional theory (DFT). Specifically, we investigate two cluster models that feature As–As bonds

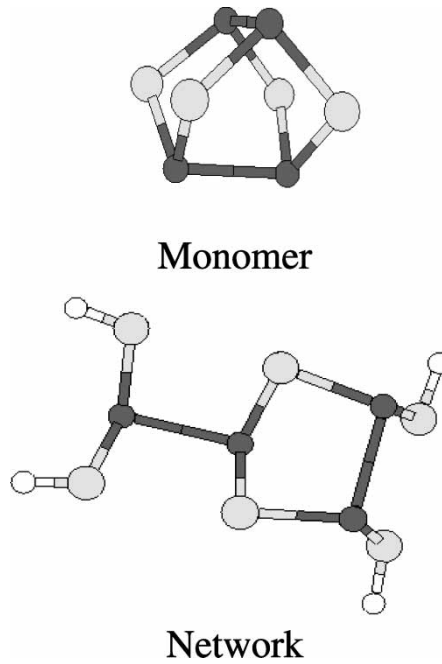

Figure 4. Cluster models of As_4S_4 in monomeric and polymeric forms. The dark atoms are As, and the light atoms are S. H atoms are used to maintain twofold coordination of S atoms in the network model.

incorporated in different ways into the glass network. The first model features the cage-like As_4S_4 unit (figure 4) that forms the basic building block of realgar. Here, the two As–As bonds are connected by four bridging S atoms to form a closed monomer unit that satisfies the valence requirements of all the atoms. In the second model, we open the monomer cage and add two more S atoms. The As dimers still share two bridging S atoms, but the bonds to the remaining S atoms mimic connections to the glass network. H atoms are used to maintain twofold coordination of the outer S atoms in this model. The electronegativity of H (2.1) is similar to that of As (2.0), so that no large unphysical charge transfers are expected owing to the S–H bonds.

The DFT calculations were carried out using a Gaussian-orbital-based methodology that has been discussed in detail elsewhere (Pederson and Jackson 1990). Pseudopotentials are used for the heavy atoms, while the H atoms are treated in an all-electron manner (Briley *et al.* 1998). The cluster models are first relaxed to a local minimum-energy configuration. The full vibrational spectrum (including frequencies and mode eigenvectors) of each model is then calculated by diagonalizing the appropriate force constant matrix. Finally, the Raman activities associated with each vibrational mode are calculated directly using the DFT (Jackson 2000), allowing us to compare and contrast the Raman signature of the two models.

In table 1 we present results for the two models shown in figure 4. The table lists all the modes in both clusters that have significant total Raman intensity in the frequency range 170–400 cm^{-1}. The Raman-active modes for both models can be grouped into a low-frequency set (180–230 cm^{-1}) and a high-frequency set (350–390 cm^{-1}). Analysis of the mode eigenvectors shows that the low-frequency

Table 1. Raman-active modes for two cluster models featuring As–As bonds. The first column identifies the model (see figure 4). The second column gives the frequencies of the Raman-active modes. The third and fourth columns give the total Raman intensities and depolarization ratios I^{HV}/I^{VV} of the modes respectively.

Cluster	ω (cm^{-1})	I^{Ram} ($Å^4\,amu^{-1}$)	ρ
Monomer	183	13.1	0.16
	221	6.7	0.06
	355	8.2	0.75
	371	49.4	0.01
Network	195	6.4	0.14
	206	6.0	0.03
	227	11.8	0.24
	351	18.0	0.33
	369	32.1	0.02
	371	33.2	0.08
	388	6.9	0.75

modes correspond mainly to As–As bond stretches, with some admixture of As–S bond bending. The high frequency modes correspond to As–S bond stretches.

The calculated Raman-active modes for the monomer model are fully consistent with the assignments made in figures 2 and 3. The low-frequency modes, at 183 and 221 cm^{-1}, are an excellent match to the positions of the strong lower-frequency peaks in the crystalline As_2S_2 spectrum and to the corresponding peaks in $As_{0.44}S_{0.56}$ glass spectrum (185 $cm^{-1}$and 220 cm^{-1} respectively). In addition, the calculated intensities (13.1 versus 6.7 for the 183 cm^{-1} and 221 cm^{-1} modes respectively) agree qualitatively with the observed intensities. This is seen most clearly in the top two curves of figure 3. The high-frequency modes of the monomer model, at 371 and 355 cm^{-1}, are also in good agreement with strong Raman peaks in the crystal and glass spectra at 361 and 346 cm^{-1} respectively. Again the calculated intensities (49.4 and 8.2 for the 371 cm^{-1} and 355 cm^{-1} modes respectively) are in good agreement with the corresponding observed intensities. The fact that the calculated positions in both cases are stiffer by about 10 cm^{-1} suggests that this shift is a systematic overestimate of the As–S bond stretch frequency by the DFT. To test this, we also computed the average stretch mode frequency for the AsS_3 pyramid, the basic building block of As_2S_3 glass. It is reasonable to expect that the calculated stretch mode for the molecular model will be near the centroid of the Raman band of the glass. The calculated symmetric stretch frequency is 362 cm^{-1}, while the centroid in the observed spectrum is near 350 cm^{-1}. Thus the DFT frequency for As–S stretches appears indeed to be somewhat stiffer than observed.

We note that the crystalline As_2S_2 Raman spectrum shown in figure 3 includes a third high-frequency peak near 350 cm^{-1} that has no analogue among the Raman-active monomer frequencies shown in table 1. We suspect that this peak corresponds to a doublet of asymmetric As–S stretch modes at 343 cm^{-1} in the isolated monomer spectrum. These modes have very little Raman intensity in the monomer model but have strong infrared intensity. Coupling between monomer units in the crystal may transfer additional Raman intensity to combinations of these modes, giving rise to the additional peak in the crystal spectrum.

The results given in table 1 show clear differences between the monomer and network models. In the low frequency range, the network model has three Raman-active modes, at 195, 206 and 227 cm^{-1}, compared with two modes in the monomer model (at 183 and 221 cm^{-1}). The network model also has an extra mode in the high-frequency range, at 388 cm^{-1}, that is not present in the monomer spectrum. The remaining high-frequency Raman-active modes are close to corresponding modes in the monomer spectrum.

In contrast with the monomer model, the calculated Raman-active modes for the network model do not agree well with the positions and intensities of peaks observed in the crystalline As_2S_2 or $As_{0.44}S_{0.56}$ glass spectra shown in figure 3. This is particularly true in the low-frequency part of the spectrum, where the network model has modes at 195 and 206 cm^{-1}. These are stiffer than the observed peak at 185 cm^{-1}. The calculated 227 cm^{-1} mode is also stiffer than the observed peak at 220 cm^{-1}. The calculated relative intensities of the network model modes (6.4, 6.0 and 11.8 for the 195 cm^{-1}, 206 cm^{-1} and 227 cm^{-1} modes respectively) also disagree with the intensities of the observed peaks, which suggest that the lower frequency modes should be more intense. Interestingly, the calculated 227 cm^{-1} mode lies near the observed peak at about 232 cm^{-1} which appears in the As_xS_{1-x} glass spectra, but not in the crystalline As_2S_2 spectrum. As seen in the inset in figure 2 (*b*), the 232 cm^{-1} peak appears at around $x = 0.35$ and grows in intensity before the 221 cm^{-1} peak appears at around $x = 0.4$. A possible interpretation is that, as x increases to 0.35, isolated As–As bonds are first formed in the glasses. The associated stretch modes are stiffer than those in monomer units and account for the observed Raman peak near 232 cm^{-1}. As the concentration of As–As bonds increases with increasing x, As_4S_4 monomer units begin to form. The Raman signature of the monomers is clearly evident at $x = 0.40$ and the monomer becomes the dominant structural motif for As–As bonds by around $x = 0.42$.

3.3. *Broken chemical order in As_2S_3 glass*

To test these ideas further, we deconvoluted the observed Raman line shape of the glasses in terms of a superposition of the requisite number of Gaussians, keeping the linewidths, centroids and intensities of each mode unrestricted. The result of the analysis appears in figure 5, in which the modes indicated with arrows and labelled R represent those of As_4S_4 monomers while the remaining modes represent those of pyramidally coordinated $As(S_{1/2})_3$ units in orpiment-like sheets. The results of figure 5 show a systematic growth in the scattering strength of R modes at the expense of O modes as the As content of glasses increases in the $0.38 < x < 0.44$ range. The deconvolution of the line shape at $x = 2/5$, has largely been made possible because of a smooth extrapolation of the Raman results of the As-rich glasses that display sharper features. In the analysis of the broad band centred at 340 cm^{-1}, we found that the relative intensities of the realgar-like modes remain relatively constant within error of measurement. The integrated area under the realgar-like Raman modes normalized to the total area, $I_R/I(x)$, is found to increase with increasing x almost linearly once $x \geqslant 0.38$ and, at $x = 2/5$, the ratio $I_R/I(x)$ acquires a value of 0.16(5).

We make use of the Raman cross-sections of the R-like and pyramidal $As(S_{1/2})_3$ modes, given by the cluster DFT calculations, and obtain a fraction of 7% of homopolar As bonds in the As_2S_3 glass. The broken chemical order inferred

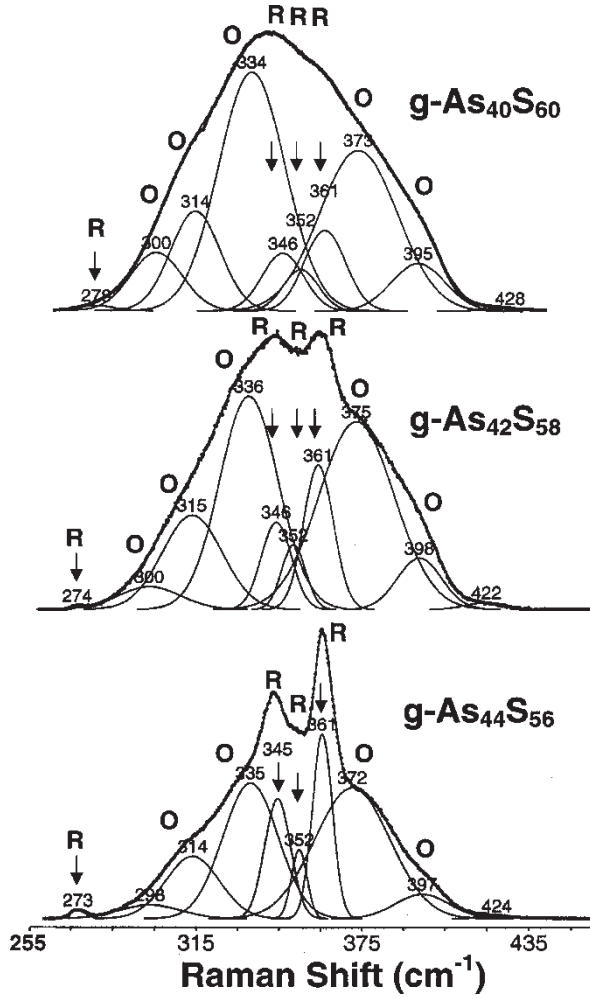

Figure 5. Raman line-shape deconvolution of the observed spectra (points) in terms of a superposition of Gaussians composed of modes of realgar (arrows) and orpiment with no restrictions on the centroid, width and intensity of each Gaussian. Note that the realgar mode scattering strengths increase with increasing x.

from Raman measurements may be compared with a value of 1% established by chemical dissolution of the glass in KOH which selectively extracts As only from As_4S_4 units (Kosek *et al.* 1983). The difference between our calculation and the result reported earlier (Kosek *et al.* 1983) is considerable. It is probably due to the over-simplified cluster models and the rather indirect procedure involved in the estimate of the Raman cross-sections.

On stoichiometric grounds, the presence of As–As bonds requires S–S bonds to occur in As_2S_3 glass. Evidence for S–S bonds in As_2S_3 glass emerged independently from ^{129}I Mössbauer spectroscopy (Zitkovsky 1989) (see also Zitkovsky and Boolchand (1989)). Here one alloys ^{129m}Te tracer and infers the chemical environment of the chalcogen parent by examining the ^{129}I nuclear hyperfine structure of the former (Boolchand 2000b). The experiments show a bimodal (A, B) site

distribution (Zitkovsky 1989, Frumar *et al.* 1997) with $I_B/I_A = 1.60(5)$. Here, the oversized ^{129m}Te tracer segregates to surfaces of large S-rich orpiment-like clusters to populate selectively the roomy and chemically disordered S–S edge sites (Phillips *et al.* 1980†, Zitkovsky 1989) (B) over the S-bridging cluster interior (A) sites. The result is a nearly seventyfold enhancement of the B over the A site population ($I_B > I_A$) which constitutes evidence for existence of internal surfaces dressing the S-rich cluster. In a homogeneous continuous random network model of As_2S_3 glass, such a large population enhancement $I_B > I_A$ would be precluded. Furthermore, the present Raman results (figure 2 (*a*)) show that the degree of nanoscale phase separation in As_2S_3 glass increases with increasing T_q as also noted in a previous study (Mamedov *et al.* 1998). The free energy of the phase separated liquid ($F = U - TS + PV$) is apparently lowered by the creation of internal surfaces that provide an additional source of enthalpy U, that is van der Waals bonding and entropy S, particularly if the clusters are small and can move, to overwhelm the endothermic reaction (Pauling 1960).

$$2(\mathrm{As-S}) \rightarrow (\mathrm{As-As}) + (\mathrm{S-S}) - 11.5\,\mathrm{kcal\,mol^{-1}} \tag{1}$$

and to promote phase separation as T_q is increased.

Unlike Raman scattering, ^{75}As nuclear quadrupole resonance (NQR) lacks the sensitivity (Taylor *et al.* 1998)† to detect the less than 2% concentration of As–As bonds in As_2S_3 glass. Furthermore, since the size of the S-rich clusters is of the order of the wavelength of visible light (as revealed by absorption band tails (Tanaka 2001)), NQR can only probe the majority (greater than 98%) As sites in the S-rich cluster interior, which are found to be orpiment like, as confirmed by the measured NQR parameters (Taylor *et al.* 1998).

3.4. *Broken chemical order and T_g maximum*

The Pauling (1960) single bond strength of a S–S bond of 50.9 kcal mol^{-1} exceeds that of an As–S bond of 47.25 kcal mol^{-1}. The increase in T_g upon alloying As in a S glass is thus qualitatively incompatible with chemical bond strength arguments (Tichy and Ticha 1995) that would require $T_g(x)$ to decrease with increasing x in the present case. T_g reflects the global connectivity of a glass network with differences in covalent bond strengths playing little role, if any, as elucidated by stochastic agglomeration theory (Micoulaut 1998) (see also Kerner and Micoulaut (1997)). According to this theory the increase in T_g upon alloying As or Ge in a Se glass reflects the increased cross-linking or connectivity of the alloyed network. The global maximum in T_g and also of liquidus T_ℓ at the stoichiometric compositions in $GeSe_2$ (Bresser *et al.* 1981) (see also Hazle and Grasseli (1986) and Cai and Boolchand (2002)) and As_2Se_3 (Georgiev *et al.* 2000) glasses is a direct consequence of nanoscale phase separation of the glass and the liquid respectively. In these systems, nanoscale phase separation effects are traced respectively to the fact that Ge–Ge bonds and

† The surface reconstruction principle proposed by Phillips *et al.* (1980) has been taken literally by Taylor *et al.* (1998). If the S-rich cluster size exceeds 100 nm, then the edge to cluster interior As site concentration ratio becomes less than 2%, and NQR measurements will be unable to probe the cluster edge As sites.

As–As bonds do not form part of the backbone once the cation concentration approaches the stoichiometric composition but nucleate separate clusters, as revealed by Raman and Mössbauer spectroscopic measurements. The lowering of T_ℓ for off-stoichiometric compositions is a natural consequence of the Born (1939) elastic shear instability (see also Jin *et al*. (2001)) owing to the presence of internal surfaces in corresponding crystals.

The reduction in T_g of an As_2S_3 glass with increasing T_q reflects the loss in global connectivity as the concentration of As_4S_4 molecules increases (figure 2(*a*)) and internal surfaces emerge. In figure 1, the sign change in the slope dT_g/dx, from a positive value at $x = 0.35$ to a negative value at $x = 0.42$, reflects the bonding role of As atoms, which serve to increase cross-linking of a S-rich ($x = 0.35$) network with the free S, but to depolymerize the network of an As-rich glass ($x = 0.42$) by clustering it. The present results thus form part of a general trend noted in the chalcogenides and has been discussed in more detail in recent reviews (Bresser *et al*. 1981, Boolchand *et al*. 2002).

3.5. *Broken chemical order and non-Arrhenius temperature variation in viscosity*

A count of Lagrangian bonding constraints (Georgiev *et al*. 2000)† shows that a network of pyramidally coordinated $As(S_{1/2})_3$ units is optimally constrained, that is three constraints per atom. SiO_2 glass, composed of a network of tetrahedral building blocks, is also optimally constrained, that is $n_c = 3$, because the bond-bending constraints associated with bridging oxygen atoms are intrinsically broken (Zhang and Boolchand 1994). If As_2S_3 glass in analogy to the optimally (Zhang and Boolchand 1994) constrained oxide glasses (SiO_2 and GeO_2) were to also form a continuous random network, liquid viscosities would display a strong behaviour, that is an Arrhenius activation with a low activation energy. Viscosities of As_2S_3 and As_2Se_3 have been measured (Phillips *et al*. 1980) and in sharp contrast with those of SiO_2 or GeO_2 melts show an Arrhenius temperature activation with a higher activation energy than in SiO_2 and GeO_2 glass. The results show that both As_2S_3 and As_2Se_3 are mildly fragile. The nanoscale phase separation of the As_2S_3 network contributes fragility (Angell 2000) that results in the observed deviation from strong behaviour for much the same reason that addition of alkali to SiO_2 disrupts the continuous random network and renders it fragile.

§ 4. Conclusions

Raman line-shape deconvolution of $As_{0.4+y}S_{0.6-y}$ glasses at $y = 0.04$, when extended to $y = 0$, show that the stoichiometric As_2S_3 glass is mildly nanoscale phase separated into small As-rich and large S-rich clusters. These results provide a structure basis to understand the local maximum in T_g, the broken chemical order inferred in earlier ^{129}I Mössbauer spectroscopy measurements, weak optical absorption tails and the non-Arrhenius temperature activation of As_2S_3 liquid viscosities and are parallel to results found on other stoichiometric chalcogenide glasses ($GeSe_2$: Boolchand and Bresser 2000, Cai and Boolchand 2002; As_2Se_3: Zitkovsky and Boolchand 1989, Georgiev *et al*. 2000).

† For an $As(S_{1/2})_3$ pyramidal unit, $2.5n_c = [n_\alpha(As) + n_\beta(As)] + 1.5[n_\alpha(S) + n_\beta(S)] = (1.5 + 3) + 1.5(2) = 7.5$ or $n_c = 3$. Here $n_\alpha = r/2$ and $n_\beta = 2r - 3$, and $r = 3$ for As and $r = 2$ for S; n_c is the count of bond-stretching (α) and bond-bending (β) constraints per atom.

Acknowledgements

We have benefited from discussions with D. McDaniel. The orpiment sample used in the present work was provided by R. Zallen. The assistance of J. Spijkerman and J. Thayer in the course of experiments is acknowledged with pleasure. The work at the University of Cincinnati was supported by National Science Foundation grant DMR 01-01808. KAJ acknowledges the support of National Science Foundation grant DMR RUI 9972333 and the President's Research Investment Fund at Central Michigan University.

References

Angell, C. A., 1988, *J. non-crystalline Solids*, **102**, 205; 1991, *ibid.*, **131–133**, 13; 2000, *Insulating and Semiconducting Glasses*, edited by P. Boolchand (Singapore: World Scientific), p. 1.

Boolchand, P., 2000a, *Asian J. Phys.*, **9**, 199; 2000b, *Insulating and Semiconducting Glasses*, edited by P. Boolchand (Singapore: World Scientific), p. 199.

Boolchand, P., and Bresser, W. J., 2000, *Phil. Mag.* B, **80**, 1757.

Boolchand, P., Georgiev, D. G., Qu, T., Wang, F., Cai, L., and Chakravarty, S., 2002, *Comptes Rendus. Chim.*, **5**, 713.

Born, M., 1939, *J. chem. Phys.*, **7**, 591.

Bresser, W. J., Boolchand, P., Suranyi, P., and DeNeufville, J. P., 1981, *Phys. Rev. Lett.*, **46**, 1689.

Briley, A., Pederson, M. R., Jackson, K. A., Patton, D. C., and Porezag, D. V., 1998, *Phys. Rev.* B, **58**, 1786.

Cai, L., and Boolchand, P., 2002, *Phil. Mag.* B, **82**, 1649.

Frumar, M., Polak, Z., Vlcek, M., and Cernosek, Z., 1997, *J. non-crystalline Solids*, **221**, 27.

Georgiev, D. G., Boolchand, P., and Micoulaut, M., 2000, *Phys. Rev.* B, **62**, R9228.

Hazle, M. A., and Grasseli, R. K., 1986, *Phys. Rev.* B, **33**, 5421.

Jin, Z. H., Gumbsch, P., Lu, K., and Ma, E., 2001, *Phys. Rev. Lett.*, **87**, 055 703.

Kawamura, H., Takasuka, T., Minato, T., Hyodo, T., and Okumura, T., 1983, *J. non-crystalline Solids*, **59–60**, 863.

Kerner, R., and Micoulaut, M., 1997, *J. non-crystalline Solids*, **210**, 298.

Kobliska, R. J., and Solin, S. A., 1973, *Phys. Rev.* B, **8**, 756.

Kosek, F., Chlebny, J., Cimpl, Z., and Masek, J., 1983, *Phil. Mag.* B, **47**, 627.

Mamedov, S., Kisliuk, A., and Quitmann, D. E., 1998, *J. Mater. Sci.*, **33**, 41.

Micoulaut, M., 1998, *Eur. Phys. J.* B, **1**, 277.

Morimoto, N., 1954, *J. Mineral* (*Sapporo*), **1**, 160.

Muniz-Miranda, M., Sbrana, G., Bonazzi, P., Menchetti, S., and Pratesi, G., 1996, *Spectrochim. Acta* A, **52**, 1391.

Myers, M. B., and Felty, E. J., 1967, *Mater. Res. Bull.*, **2**, 535.

Pauling, L., 1960, *Nature of the Chemical Bond* (Ithaca, New York: Cornell University Press), p. 85.

Pederson, M. R., and Jackson, K. A., 1990, *Phys. Rev.* B, **41**, 7453.

Phillips, J. C., Beavers, C. A., and Gould, E. B., 1980, *Phys. Rev.* B, **21**, 5724.

Renninger, A. L., and Averbach, B. L., 1973, *Acta crystallogr.* B, **29**, 1583.

Shimakawa, K., Yoshida, N., Ganjoo, A., Kuzukawa, A., and Singh, J., 1998, *Phil. Mag. Lett.*, **77**, 153.

Tanaka, K., 1989, *Phys. Rev.* B, **39**, 1270.

Tanaka, K., Gohda, S., and Odajima, A., 1985, *Solid St. Commun.*, **56**, 899.

Tanaka, K. E., 2001, *J. Optoelectron. Adv. Mater.*, **3**, 189.

Taylor, P. C., Hari, P., Kleinhammes, A., Kuhns, P. L., and Moulton, W. G., 1998, *J. non-crystalline Solids*, **227–230**, 770.

Tichy, L., and Ticha, H., 1995, *J. non-crystalline Solids*, **189**, 141.

Vinogradova, G. Z., Dembovskii, S. A., Kuzmina, T. N., and Chernov, A. P., 1967, *Russ. J. inorg. Chem.*, **12**, 1715.

WAGNER, T., KASAP, S. O., VLCEK, M., SKLENAR, A., and STRONSKI, A., 1998, *J. Mater. Sci.*, **3**, 5581.
WARD, A. T., 1968, *J. phys. Chem.*, **72**, 4133.
YANG, C. Y., SAYERS, D. E., and PAESLER, M., 1987, *Phys. Rev.* B, **36**, 8122.
ZALLEN, R., 1974, *Phys. Rev.* B, **9**, 4485.
ZALLEN, R., and LUCOVSKY, G., 1976, *Selenium*, edited by R. A. Zingaro and W. C. Cooper (New York: Van Nostrand Reinhold), p. 148.
ZALLEN, R., and SLADE, M. L., 1974, *Phys. Rev.* B, **9**, 1627.
ZHANG, M., and BOOLCHAND, P., 1994, *Science*, **266**, 1355.
ZITKOVSKY, I., 1989, PhD Thesis, University of Cincinnati, Cincinnati, Ohio, USA.
ZITKOVSKY, I., and BOOLCHAND, P., 1989, *J. non-crystalline Solids*, **114**, 70.